T CELL ACTIVATION

Mitochondria maintain controlled activation state of epithelial-resident T lymphocytes

Špela Konjar[1,2]*, Ulrika C. Frising[2]*, Cristina Ferreira[1,2], Reinhard Hinterleitner[3,4], Toufic Mayassi[3,4], Qifeng Zhang[2], Birte Blankenhaus[1], Nejc Haberman[5], Yunhua Loo[2], Joana Guedes[2], Marta Baptista[1], Silvia Innocentin[2], Joerg Stange[2], Douglas Strathdee[6], Bana Jabri[3,4], Marc Veldhoen[1,2†]

Epithelial-resident T lymphocytes, such as intraepithelial lymphocytes (IELs) located at the intestinal barrier, can offer swift protection against invading pathogens. Lymphocyte activation is strictly regulated because of its potential harmful nature and metabolic cost, and most lymphocytes are maintained in a quiescent state. However, IELs are kept in a heightened state of activation resembling effector T cells but without cytokine production or clonal proliferation. We show that this controlled activation state correlates with alterations in the IEL mitochondrial membrane, especially the cardiolipin composition. Upon inflammation, the cardiolipin composition is altered to support IEL proliferation and effector function. Furthermore, we show that cardiolipin makeup can particularly restrict swift IEL proliferation and effector functions, reducing microbial containment capability. These findings uncover an alternative mechanism to control cellular activity, special to epithelial-resident T cells, and a novel role for mitochondria, maintaining cells in a metabolically poised state while enabling rapid progression to full functionality.

INTRODUCTION

The epithelia are the largest potential port for microbial invasion, especially the intestines, which harbor up to 100 trillion microorganisms (*1*). The intestines, essential to absorb nutrients, need to balance the maintenance of beneficial microbes yet offer robust protection against invasion, avoiding tissue damage. The intestines have at least two anatomically distinct immune compartments, the intraepithelial lymphocytes (IELs) residing between the epithelial cells of the villi and the deeper layer of lamina propria lymphocytes (*2*). Intestinal IELs are composed of two main subsets, natural and induced T cells (*3*). Induced IELs express CD8αβ and T cell receptor (TCR) αβ and are part of an important memory population of tissue-resident memory (T_{RM}) cells. Natural IELs express either the TCR composed of the γδ chains or the TCRαβ in association with CD8αα homodimers. IELs are found at the barrier site, providing regional immune surveillance and protection against reinfection (*4*). IELs do not recirculate (*5*) and have reciprocal interactions with intestinal epithelial cells with which they contribute to tissue homeostasis. Thus, the maintenance of IELs is of importance to preserve a healthy epithelial barrier.

Upon activation, a limited number of precursor T cells proliferate rapidly, gaining the ability to kill target cells and secrete cytokines such as tumor necrosis factor (TNF) and interferons (IFNs) (*6*). Proliferation ensures that sufficient numbers of T cells migrate throughout the body to remove infected cells and pathogens (*7*). Quiescent lymphocytes, which do not undergo clonal division or secrete substantial amounts of soluble factors, have limited metabolic needs. They make optimal use of available carbons by using oxidative phosphorylation, obtaining maximum energy without diverting resources to the generation of biomolecules. Activated lymphocytes proliferate, differentiate, and require large amounts of energy and biomolecules. The effector phase is not sustained, and most effector cells die in a contraction phase with some acquiring a quiescent metabolic state (*8*). This enables long-term maintenance of memory cells, which have the potential to increase their metabolism faster than naive cells (*9*).

Most T lymphocytes, such as IELs, are tissue-resident, with properties that are not typical of memory or effector T cells. Intestinal IELs share characteristics with effector memory T cells, expressing CD44 and low levels of CD62L. IELs express early activation markers, contain cytolytic and microbicidal proteins, and have the capacity to release cytokines (*10*). However, despite having these effector-like properties, IELs are arrested in a poised activation state, are long-lived, and are oligoclonal (*10*–*12*), characteristics shared with memory T cells. IELs are metabolically prepared for action, containing high levels of mRNA for metabolic enzymes, particularly of those involved in lipid metabolism (*13*, *14*). The epithelia are lipid-rich, which may provide a readily available source of nutrients for IELs (*15*), which express surface molecules involved in lipid uptake (*13*). Skin T_{RM} cells use lipids via intracellular transport including fatty acid–binding proteins 4 and 5, supporting their longevity and protective function (*16*).

The increased presence of receptors and enzymes involved in metabolism compared with conventional T cells suggests that altered metabolism may contribute to IEL maintenance. It remains to be determined whether altered lipid metabolism sets IELs apart from conventional T cells or whether it reflects their semi-activation status. Acetyl-CoA (coenzyme A) generated during glycolysis can be used in de novo fatty acid synthesis and may be stored for future use in fatty acid oxidation (FAO), supporting memory T cell differentiation (*17*). In this study, we assessed the poised activation status of IELs and whether increased transcripts of metabolic enzymes are unique to IELs. We show that increased metabolic potential is shared with recently activated T cells, reflecting the semi-activation status of IELs. We uncovered that IELs are metabolically arrested from progressing to full activation and show an altered mitochondrial lipid makeup,

[1]Instituto de Medicina Molecular, Faculdade de Medicina da Universidade de Lisboa, Avenida Professor Egas Moniz, Lisbon, 1649-028, Portugal. [2]Babraham Institute, Babraham Research Campus, Cambridge CB22 3AT, UK. [3]Department of Medicine, University of Chicago, 900 East 57th Street, MB#9, Chicago, IL 60637, USA. [4]Committee on Immunology, University of Chicago, Chicago, IL 60637, USA. [5]Department of Molecular Neuroscience, University College London Institute of Neurology, Queen Square, London WC1N 3BG, UK. [6]Beatson Institute for Cancer Research, Garscube Estate, Glasgow G61 1BD, Scotland.
*These authors contributed equally to this work.
†Corresponding author. Email: marc.veldhoen@medicina.ulisboa.pt

the cardiolipins (CLs). We correlate the activation status of IELs with alterations in CL makeup and demonstrate the particular importance of mitochondria alterations, especially CL composition, in IEL activation compared with conventional T cells.

RESULTS

IELs have enhanced metabolic and cytotoxic potential

Intestinal IELs consist largely of $CD8^+$ T cells. To define IELs for this study, we used $CD8\alpha^+$ lymphocytes from 8- to 12-week old C57BL/6J mice. In line with previous studies, intestinal IELs express the tissue-resident integrin CD103 (integrin αE) (*18*) and the C-type lectin CD69 (*13*). Antibody staining for CD8α, CD69, CD62L, and CD103 of lymphocytes sourced from the intestinal intraepithelial fraction provides a homogeneous IEL cell population, in contrast to $CD8^+$ T cells found in secondary lymphoid organs (fig. S1, A to C) (*13*).

Altered metabolic pathways may set IELs apart from other lymphocytes not undergoing clonal expansion, naive and memory T cells. Upon analysis of the transcriptional profile of small intestinal $CD8^+$ IELs, we confirmed increased expression of metabolic enzymes involved in lipid uptake and metabolism in IELs compared with $CD44^{hi}CD8^+$ memory T cells (*13*, *14*). This was particularly the case for enzymes involved in the mevalonate, lanosterol, and cholesterol synthesis pathways, suggesting increased lipid metabolite generation (Fig. 1A). Lipid staining indicated increased presence of lipid metabolites stored in droplets in IELs compared with similar nonproliferating naive and memory $CD8^+$ T cells (Fig. 1, B and C). However, increased lipid metabolism is a consequence of the activation status of IELs, because stimulation of naive $CD8^+$ T cells resulted in lipid droplet generation (Fig. 1D) (*19*).

Differential gene expression and flow cytometry analysis of IELs showed strong predisposition to cytotoxic potential with high levels of intracellular lysosomal-associated membrane protein-1(LAMP-1; CD107a), lysosomal compartment, and lytic effector molecules such as granzymes (Fig. 2, A to C, and fig. S2A). Electron microscopy (EM) analysis revealed dark granular structures previously identified as secretory granules or lysosomes (Fig. 2D) (*20*).

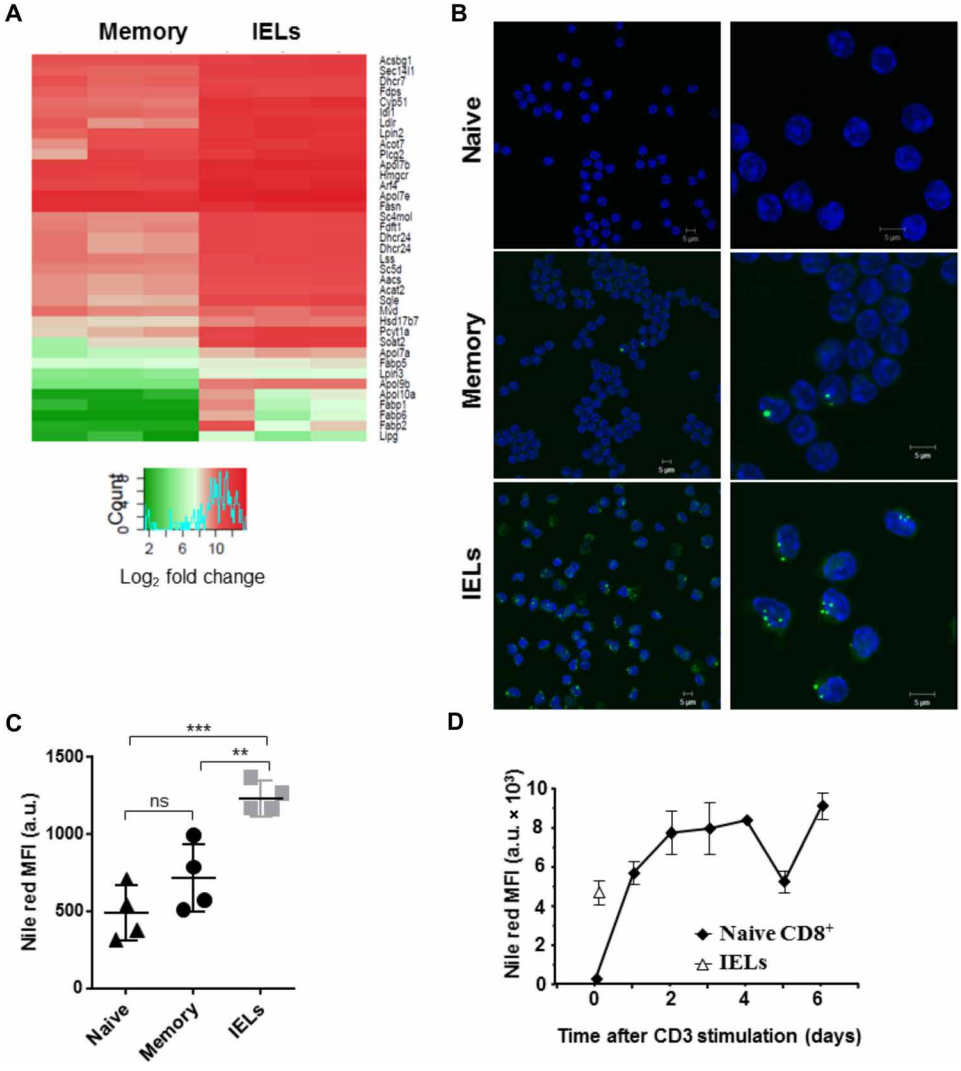

Fig. 1. IELs have a heightened metabolic state. (**A**) Memory $CD8^+$ T cells from spleen or intestinal IEL fraction were isolated by flow-sorting (purity, >98%) and differential expression (DESeq) analysis of gene expression was performed. Heatmap of normalized gene expression of differentially expressed mRNAs associated with lipid metabolism is shown ($n = 3$). (**B** and **C**) Flow-sorted $CD8^+$ T cells sourced from the spleen ($CD44^{lo}$, naive; $CD44^{hi}$, memory) or intestinal IEL fraction were stained with Nile Red. Cells were analyzed by (B) fluorescence microscopy counterstained with DAPI in blue. Representative overview (left column) and closeup (right column) pictures of more than four biological repeats, or (C) flow cytometry ($n = 4$) for mean fluorescence intensity (MFI) of Nile Red. a.u., arbitrary units; ns, not significant. Scale bars, 5 μm. (**D**) Naive $CD8^+$ T cells were purified by magnetic cell sorting and stimulated with plate-bound anti-CD3/CD28 for 2 days, cells were maintained in IL-2 (diamonds) and analyzed daily by flow cytometry, and Nile Red fluorescence intensity levels were plotted ($n = 3$; three samples were analyzed in this experiment shown, representative of three biological repeats). Ex vivo isolated IELs (triangle) assessed on the same day are shown. For statistical analysis, one-way ANOVA with multiple comparison test was used. Error bars indicate SDs. $^{**}P < 0.01$, $^{***}P < 0.001$.

IEL activation is curtailed

Our data confirmed that IELs are in a heightened state of activation comparable with recently activated effector $CD8^+$ T cells (*21*). Yet, IEL populations, like those in the epidermis, which are only generated during a narrow time window in the embryonic thymus (*22*), are maintained in this heightened metabolic state over a long time in contrast to effector T cells (fig. S3, A and B). The long-term maintenance of IELs suggests that they are metabolically fit and could undergo mitochondrial biogenesis similar to memory $CD8^+$ T cells (*23*). EM analysis detected mitochondria in IELs at increased numbers compared with naive T cells (Fig. 3A and fig. S3C).

Extracellular flux analysis was used to test the metabolic capacity of $CD8^+$ T cell subsets. All cell populations exhibited a similar basal oxygen consumption rate (OCR) (Fig. 3B and fig. S3D). Consistent with published data (*23*), memory $CD8^+$ T cells showed an enhanced

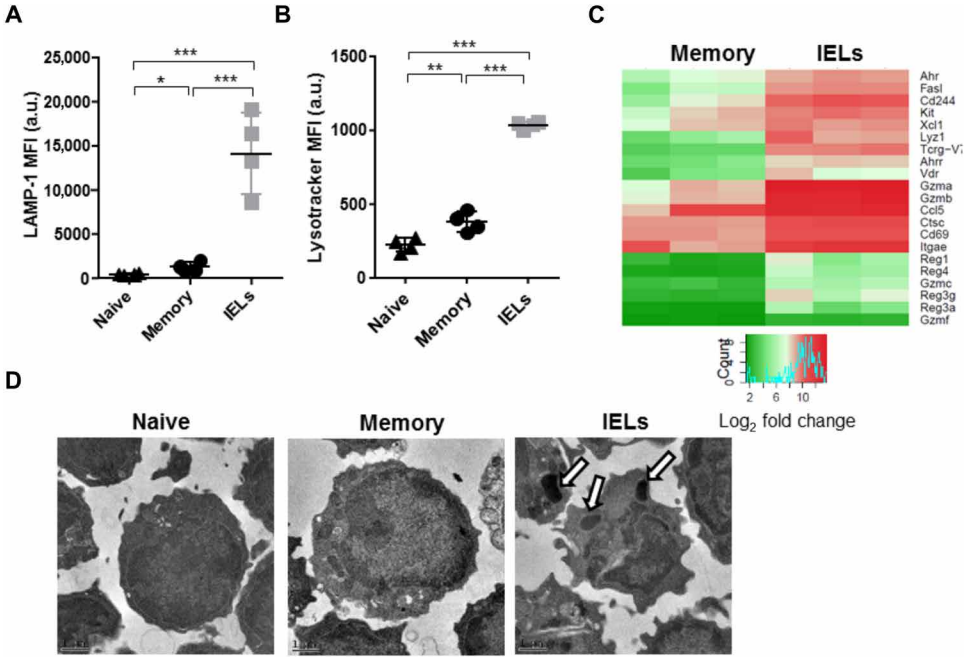

Fig. 2. IELs are in heightened activation state. (**A** and **B**) CD8$^+$ T cells obtained from the spleen (CD44^{lo}, naive; CD44^{hi}, memory) or small intestinal IEL fraction were stained intracellular for (A) LAMP-1 (CD107a) and (B) Lysotracker (n = 4). MFIs are shown. (**C**) Differential expression (DESeq, Negative Binomial Distribution) analysis comparing flow cytometry–sorted spleen sourced CD8$^+$ memory cells (CD44^{hi}) and small intestinal CD8$^+$ IELs. Heatmap of normalized gene expression of genes associated with cytotoxic potential in T cells is shown (n = 3). (**D**) Representative EM pictures of flow-sorted CD8$^+$ T cells; naive and memory T cells from the spleen and IELs. Indicated with arrows are secretory granules. For statistical analysis, one-way ANOVA with multiple comparison test was used. Error bars indicate SDs. *P < 0.05, **P < 0.01, ***P < 0.001.

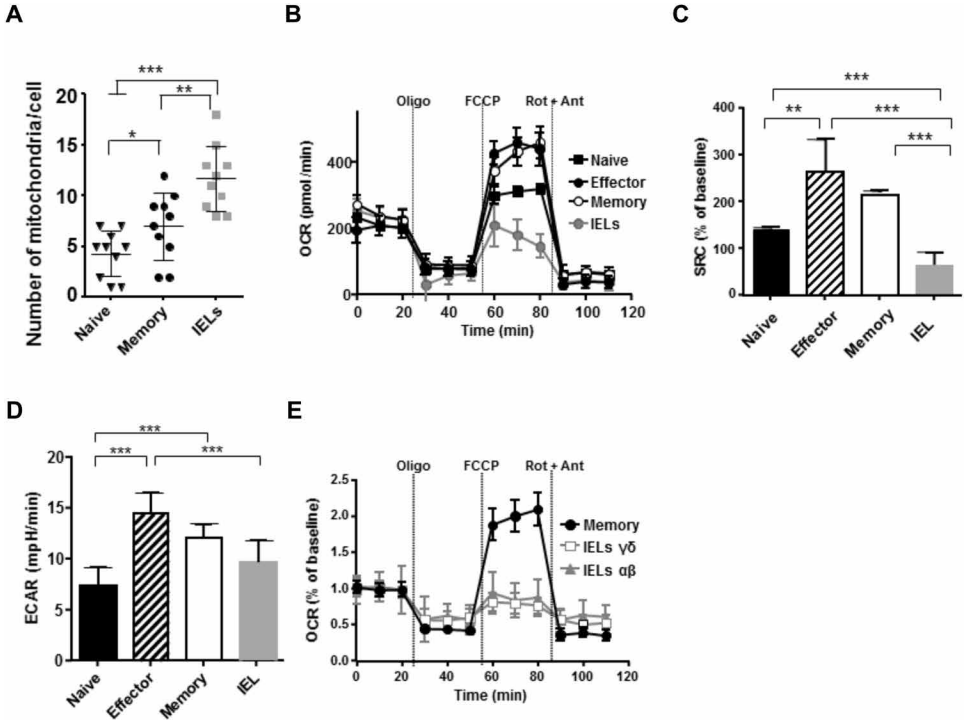

Fig. 3. IELs are metabolically arrested. (**A**) Flow-sorted CD8$^+$ T cells were processed for imaging with TEM, and the number of mitochondria per cell was quantified (n = 10). (**B** to **E**) Naive CD8$^+$CD44^{lo} or memory CD8$^+$CD44^{hi} T cells obtained from spleens and IELs obtained from the small intestine were flow-sorted (>98% purity) and assessed on a Seahorse analyzer. (B) Extracellular flux analysis comparing CD8$^+$ T cell subsets sourced from the spleen (CD44^{lo}, naive; CD44^{hi}, memory; naive T cells after 24 hours of anti-CD3/CD28 stimulation, effector) and IELs from the small intestine. OCR is plotted against time under basal conditions and in response to indicated chemicals. Oligo, oligomycin; Rot, rotenone; Ant, antimycin A. (C) SRC (maximum OCR/baseline OCR) for indicated cell subsets. (D) ECAR for indicated CD8$^+$ T cell populations. (E) As described in (B), but upon flow-sorting of the two major IEL populations, via negative sorting based on TCR identity, TCRαβ or TCRγδ T cells were assessed separately compared with memory T cells. Data are representative of at least two experiments performed in triplicate. For statistical analysis, one-way ANOVA with multiple comparison test was used. Error bars indicate SDs. *P < 0.05, **P < 0.01, ***P < 0.001.

mitochondrial OCR and markedly increased spare respiratory capacity (SRC; the ratio between maximal OCR and basal OCR) compared with naive CD8$^+$ T cells (Fig. 3C). Because IELs are partially activated (*21*), we also assayed recently activated effector T cells. After 24 hours in vitro anti-CD3/CD28 stimulation, these cells express high levels of CD69 comparable with IELs, use aerobic glycolysis measured by the extracellular acidification rate (ECAR) (Fig. 3D), a consequence of lactic acid production, and show a strong SRC (Fig. 3, B and C). In contrast, IELs, expressing either TCRγδ or TCRαβ, showed no SRC compared with other CD8$^+$ T cells tested (Fig. 3, B and E). IELs did not show an OCR above basal levels to increasing concentrations of the mitochondrial uncoupler carbonilcyanide *p*-triflouromethoxyphenylhydrazone (FCCP) (fig. S3, E to G). Despite the controlled activation state and increased

mitochondrial presence, IEL metabolic capacity does not resemble that of effector or classic memory T cells.

Diminished mitochondrial MitoTracker binding in IELs

The low SRC of IELs could not be explained by a decrease in mitochondrial numbers (Fig. 3A). Thus, we explored the state of the mitochondria using MitoTracker Green, a carbocyanine-based probe that localizes to mitochondria (*23*, *24*). The mitochondria lined the cytoplasm of naive T cells and were often found in clusters in memory T cells. Despite the increase in the number of mitochondria (Fig. 3A and fig. S3C), MitoTracker staining was markedly reduced in IELs compared with other $CD8^+$ T cells (Fig. 4, A and B). The use of MitoTracker Deep Red resulted in a similar profile (fig. S4A), but antibody staining against the outer mitochondrial membrane protein Tom20 did not show an altered staining profile between $CD8^+$ T cells from the spleen and IELs (fig. S4B).

Low mitochondrial staining in IELs was not due to cell activation. Stimulated $CD8^+$ T cells maintained a strong staining over time (Fig. 4C). However, we observed reduced mitochondrial membrane potential in IELs compared with splenic $CD8^+$ T cells (Fig. 4D and fig. S4, C and D), with similar limited mitochondrial reactive oxygen species (ROS) production in all nonproliferating T cell subsets but with lower cellular ROS levels observed in IELs compared with memory $CD8^+$ T cells (Fig. 4, E and F, and table S1). This suggested that reduced mitochondrial detection with MitoTracker dyes could result from altered mitochondrial membrane modifications specific to IELs (*25*).

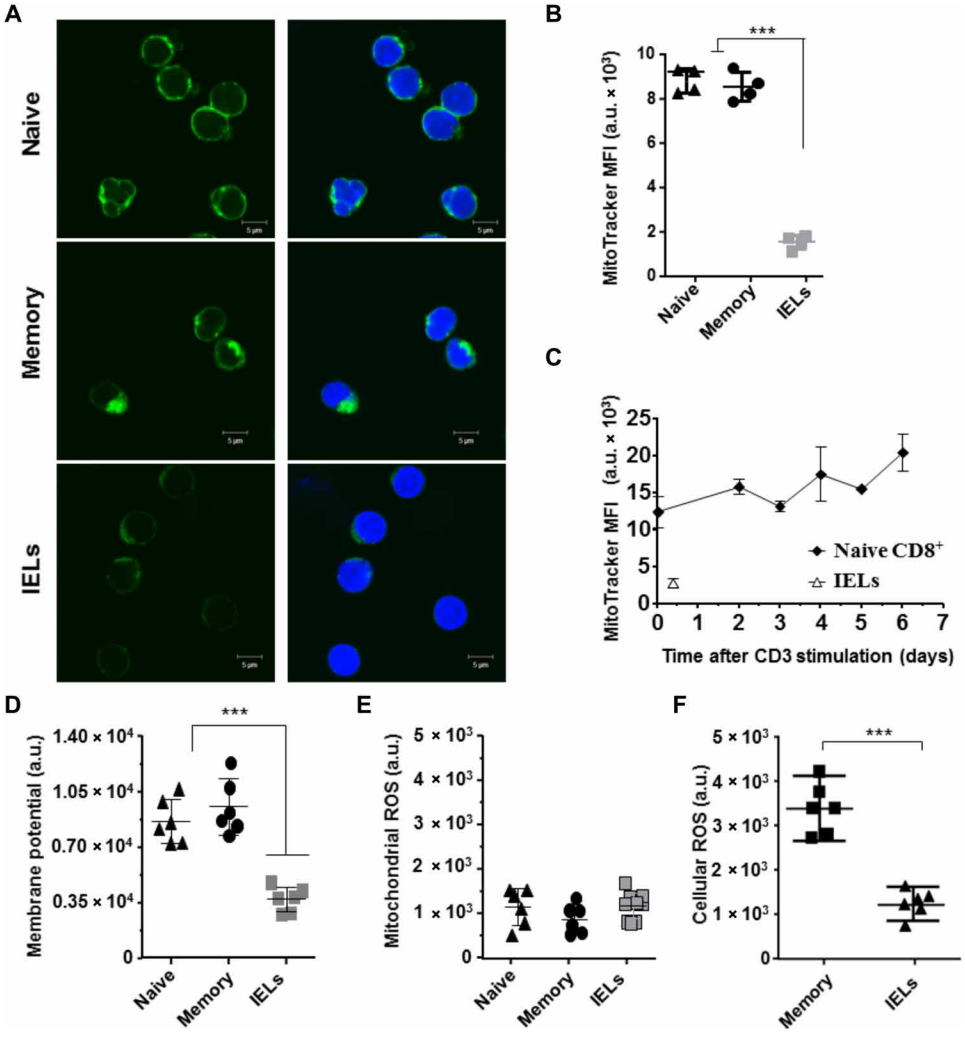

Fig. 4. IELs have altered mitochondria. (**A** and **B**) Flow-sorted $CD8^+$ T cells sourced from the spleen ($CD44^{lo}$, naive; $CD44^{hi}$, memory) or the small intestinal IEL fraction were stained with MitoTracker Green. Cells were analyzed by (A) fluorescence microscopy counterstained with DAPI in blue (representative picture of four independent biological repeats) or (B) flow cytometry ($n = 3$ to 4) for MFI of MitoTracker Green. Scale bars, 5 μm. (**C**) Naive $CD8^+$ T cells were purified by magnetic cell sorting and stimulated with plate-bound anti-CD3/CD28 for 2 days, and cells were maintained in IL-2 (diamonds). Cells were analyzed daily by flow cytometry, and MitoTracker fluorescence intensity levels were plotted. Freshly obtained intestinal IELs were analyzed simultaneously ($n = 3$; three biological repeats), and average values were plotted as a triangle. (**D** to **F**) Mitochondrial membrane potential (MTO M7510) (D) (pooled data from two experiments with $n = 3$), mitochondrial (MitoSOX) (E), or total cellular (H_2DCFDA) ROS production (F) (pooled data from two experiments with $n = 2$ to 3). For statistical analysis, one-way ANOVA with multiple comparison test was used. Error bars indicate SDs. ***$P < 0.001$.

Low mitochondrial staining in IELs was not due to cell activation. Stimulated $CD8^+$ T cells maintained a strong staining over time (Fig. 4C). However, we observed reduced mitochondrial membrane potential in IELs compared with splenic $CD8^+$ T cells (Fig. 4D and fig. S4, C and D), with similar limited mitochondrial reactive oxygen species (ROS) production in all nonproliferating T cell subsets but with lower cellular ROS levels observed in IELs compared with memory $CD8^+$ T cells (Fig. 4, E and F, and table S1). This suggested that reduced mitochondrial detection with MitoTracker dyes could result from altered mitochondrial membrane modifications specific to IELs (*25*).

Mitochondrial status correlates with IEL activity

IELs cannot be maintained in steady state in vitro. Adoptive IEL transfer into a lymphopenic host showed a robust MitoTracker staining accompanied by increased cell proliferation (Fig. 5A), suggesting that IEL mitochondrial membranes are altered upon activation. To prompt the effector function of IEL in protecting small intestinal epithelium, we infected mice with the small intestinal parasite *Eimeria vermiformis* (Ev) (*26*, *27*). This resulted in increased MitoTracker staining in ileum-sourced IELs; increased IEL numbers; and increased mitochondrial ROS, IFNγ, and TNF production (Fig. 5B and fig. S5, A to D). IELs showed similar enhanced mitochondrial detection in interleukin-22 (IL-22)–deficient mice, in which barrier protection is compromised so that immune cells get increased exposure to microorganisms (*28*). The detection of IEL mitochondria in IL-22–deficient mice returned to steady-state levels upon antibiotic-mediated bacterial depletion (Fig. 5C). Injection of anti-CD3ε, resulting in activation of all T cells, was sufficient to increase mitochondrial staining and proliferation of TCRαβ and TCRγδ IEL populations (Fig. 5, D to H). Upon activation, mitochondrial membrane potential was increased in IELs compared with steady state (Fig. 5I). These data indicate that MitoTracker-based mitochondrial staining is an indicator of the IEL activation status.

IEL mitochondria have different CL composition

EM analysis revealed reduced mitochondrial surface area in IELs, indicating potential alterations at the mitochondrial

level (Fig. 6A). CLs are phospholipids found exclusively in mitochondria, strongly associated with membranes in which proteins of the electron transport chain are located, essential for the optimal function of enzymes involved in mitochondrial energy metabolism (*29*, *30*). Absence of CLs does not reduce basal oxidative phosphorylation rate but results in significant uncoupling at higher rates of respiration (*31*). The use of 10-*N*-nonyl acridine orange (NAO), the fluorescence of which is associated with the organization of the mitochondrial membrane (*32*), suggested altered CL content, organization, or composition in IELs compared with splenic $CD8^+$ T cells (Fig. 6B). The NAO staining intensity did not change upon IEL activation (Fig. 6C). CL analysis by mass spectrometry in highly pure (>98%) $CD8^+$ T cell subsets found that memory $CD8^+$ T cells contained more CL than naive $CD8^+$ T cells, with IELs containing twice the amount of CLs per cell compared with naive T cells (Fig. 6D).

CL species are key modulators of mitochondrial proteins, and their composition varies between cell types (fig. S6A) (*33*). The diversity in species is regulated by differences in CL synthesis, catabolism, and remodeling, potentially incorporating four different acyl residues (*34*). The acyl chain composition is important for inner membrane fluidity, structure, and osmotic stability. In addition, the affinity of CL to mitochondrial inner membrane proteins affects functional properties of proteins (*30*, *35*), such as activity of mitochondrial respiratory chain complexes (*36*). Lymphocyte mitochondrial membranes have a varied CL makeup compared with the heart, with acyl moieties that have 72 or 74 carbons most common (fig. S6, A and B) (*29*). The major CL species composition of peripheral $CD8^+$ T cells is similar, but for 72-6 levels, it was found to be more abundant in memory T cells (fig. S6B). The CL composition in IELs showed marked alterations compared with splenic T and B cells. IELs have reduced levels of the canonical 72-6, 72-7, 74-7, and 74-8 CL species, whereas the contribution of more unsaturated CLs 72-9, and especially the longer 74-10 and 76-12, is markedly increased (Fig. 6E and fig. S6B). Collectively, these data suggested that altered mitochondrial function, possibly due to altered fatty acyl chain composition of CLs and membrane structure, might play a role in arresting IELs in a controlled activation state, enabling basal respiration and surveillance activity but without effector functions.

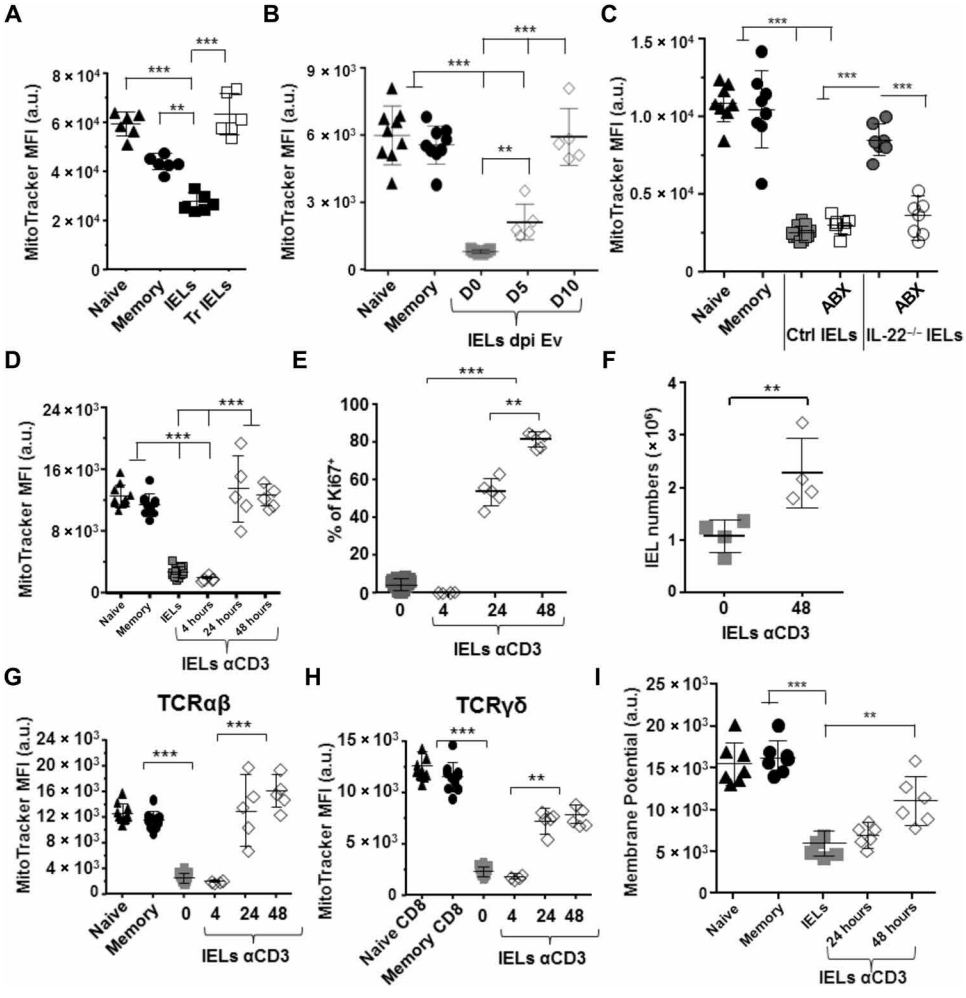

Fig. 5. IEL mitochondrial staining correlates with activation. (**A**) IELs were purified by flow cytometry and transferred intravenously into lymphopenic hosts. After 6 weeks, MitoTracker Deep Red–based detection of mitochondria was performed in indicated cell populations [trIELs (transferred IEL)] (pooled data from two experiments with $n = 3$). (**B**) C57BL/6 mice were infected intragastrically with 1000 *E. vermiformis* oocysts, and MitoTracker Green–based detection of mitochondria was performed on IELs harvested at indicated time points after infection from the ilea ($n = 5$). dpi, days post infection. (**C**) IELs were purified from control mice and IL-22–deficient mice treated or not with broad-spectrum antibiotics (ABX) and mitochondria assessed with MitoTracker Green (pooled data from two experiments with $n = 4$). (**D** to **I**) C57BL/6 mice were intraperitoneally injected with anti-CD3, and (D) MitoTracker Green–based detection of mitochondrial mass was assessed at indicated time points (pooled data from three experiments with $n = 2$ to 3). (E) Proportion of IELs positive for Ki67 and (F) number of T cells by flow cytometry analysis at indicated time points after anti-CD3 administration (representative of three biological repeats, $n = 4$ to 5). MitoTracker Green–based detection of mitochondria was performed in indicated cell populations, naive and memory $CD8^+$ cells from the spleen, and TCRαβ (G) and TCRγδ (H) IELs isolated from the small intestine at indicated time points after anti-CD3 injection (representative of more than three biological repeats, $n = 5$ to 10). (I) Mitochondrial membrane potential (MTO M7510) on indicated $CD8^+$ T cell populations at indicated time points after anti-CD3 injection (pooled data from two experiments). One-way ANOVA with multiple comparison test was used. Error bars represent SDs. $^{**}P < 0.01$, $^{***}P < 0.001$.

Alterations in CLs correlate with IEL activation

To correlate the alterations in mitochondria with IEL effector functions, we infected mice with Ev parasites and assessed MitoTracker staining with IEL proliferation, mitochondrial ROS production, and the production of IFNγ and TNF. The increased MitoTracker staining correlated strongly with IEL effector function: increased proliferation, accumulation of IELs at the site of infection, and the production of IFNγ and TNF (Fig. 7, A to D).

Upon flow-sorting of IELs (>98% purity) from control or Ev-infected animals based on the MitoTracker staining (fig. S7A), we assessed CL species distribution. Activated IELs showed a CL profile

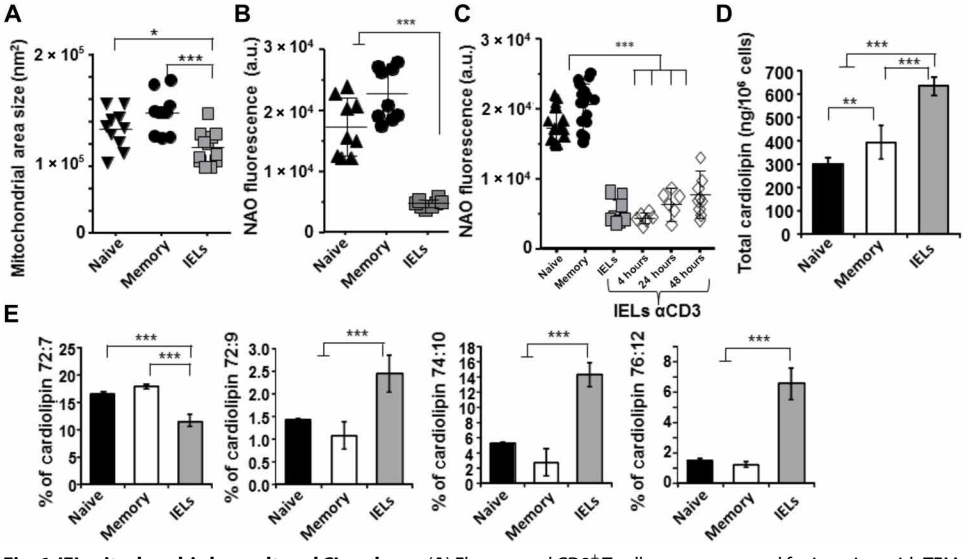

Fig. 6. IEL mitochondria have altered CL makeup. (**A**) Flow-sorted CD8$^+$ T cells were processed for imaging with TEM, and mitochondrial surface area was determined for each mitochondrion within a given cell. Data are represented as an average for mitochondrial surface area on a per-cell basis (n = 10 naive cells, n = 10 memory cells, and n = 12 IELs). (**B** and **C**) CD8$^+$ T cells from spleen or intestinal IELs were stained with NAO in (B) steady state (n = 3 from three biological repeats) or (C) indicated CD8$^+$ T cell populations at indicated time points after anti-CD3 injection (pooled data from three experiments with n = 2 to 3). (**D** and **E**) Flow-sorted naive and memory CD8$^+$ T cells, as well as IELs, were analyzed by mass spectrometry for (D) their total CL content (n = 9) or (E) the relative contribution of selected CL species (n = 8). One-way ANOVA with multiple comparison test was used. Error bars represent SDs. *P < 0.05, **P < 0.01, ***P < 0.001.

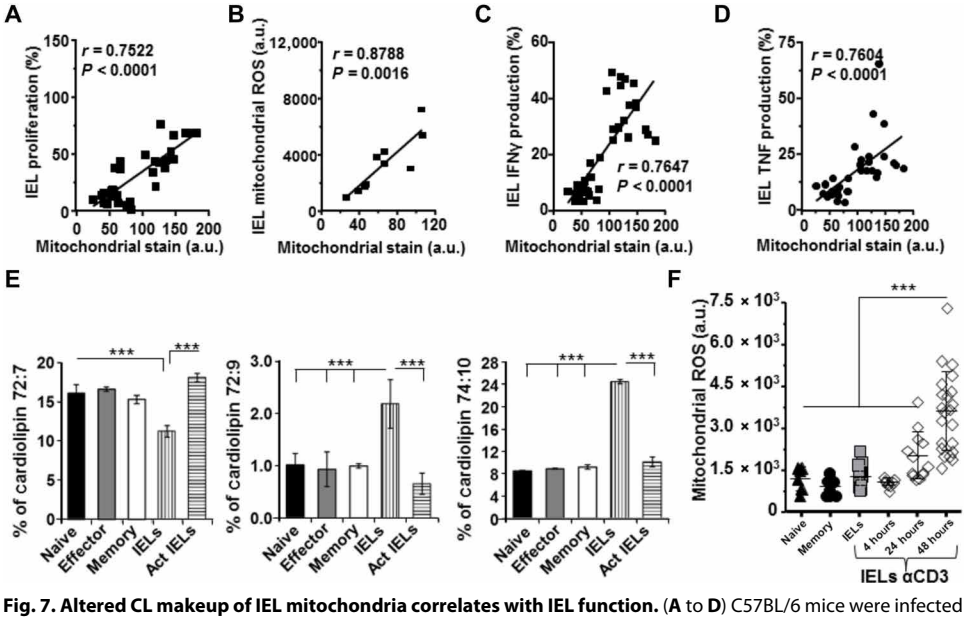

Fig. 7. Altered CL makeup of IEL mitochondria correlates with IEL function. (**A** to **D**) C57BL/6 mice were infected intragastrically with 1000 *E. vermiformis* oocysts, and MitoTracker Green–based detection of mitochondria was performed on ilea-sourced IELs harvested 10 days after infection (≥4 biological repeats, $n \geq 2$ per experiment) or from uninfected controls. MFI of MitoTracker Green staining was plotted (x axis) against (A) Ki67, (B) mitochondrial ROS production, and (C) proportion of IFNγ or (D) TNF production. (**E**) Mass spectrometry analysis of the relative contribution of selected CL species detected in indicated CD8$^+$ T lymphocytes (n = 4 to 5). Act, activated. (**F**) ROS production by MitoSOX staining was performed on mice injected with anti-CD3 at indicated time points (pooled data from three experiments with $n \geq 3$). For statistics, linear regression was used for (A) to (D) and one-way ANOVA with multiple comparison test was used for (E) and (F). Error bars represent SDs. ***P < 0.001.

similar to that observed for splenic CD8$^+$ T cells, in marked contrast to steady-state IELs (Fig. 7E and fig. S7B). We found mitochondrial ROS production in in vivo activated IELs, with anti-CD3 or upon Ev infection (Fig. 7F and fig. S5B), but only after mitochondrial mass detection and membrane potential were increased (Fig. 5, D and I). This shows that the acyl chain CL composition is changed in activated IELs, associated with the unleashing of their effector functions.

CL composition affects IEL function

CLs are an important component for the optimal activity of proteins regulating oxidative phosphorylation (*30*) and have recently been shown to specifically but intermittently interact with adenosine 5′-triphosphate (ATP) synthase, determining its assembly and function (*37*). In Barth syndrome, mutations in the *tafazzin* (*Taz*) gene result in altered CL composition and levels (*38*). Tafazzin transfers acyl chains to and from phospholipids to generate CLs. It targets curved lipid bilayers that have a higher structural order, thereby contributing to mitochondrial cristae (*39*). To test the direct effect of CLs on IELs, which express high levels of *Taz* (fig. S8A), we used *Taz*-deficient mice that show a similar alteration in CLs as found in Barth syndrome patients (*40*, *41*). To limit the absence of Taz to immune cells, we generated bone marrow chimeric mice using Rag2-deficient mice as hosts. *Taz*-deficient bone marrow chimeric mice had similar numbers of lymphocytes in the small intestine compared with those receiving control *Taz*-sufficient bone marrow (fig. S8B).

MitoTracker staining was similarly low in IELs from wild-type control and *Taz*-deficient bone marrow chimeras (Fig. 8A). Anti-CD3 activation increased MitoTracker staining in control IELs, as reported before. In contrast, *Taz*-deficient IELs showed a markedly reduced rise in staining intensity (Fig. 8A). Upon activation, splenic T cells displayed indiscriminate proliferation between wild-type and *Taz*-deficient CD8 T cells (Fig. 8B), yet Taz-deficient IELs showed significantly reduced proliferation at both 24 and 48 hours after stimulation (Fig. 8C). To assess the relevance of the reduced activation of IELs, we infected Rag2-deficient mice reconstituted with either wild-type or *Taz*-deficient bone marrow with Ev.

Taz-deficient animals showed a markedly higher parasite burden from day 8 to day 10 compared with *Taz*-sufficient controls (Fig. 8, D and E). At day 10, we assayed the cellular composition of the ileum IELs. We noted an increase in CD8αβ and $CD4^+$ T cell proliferation, which migrate to the IEL compartment during inflammation (*42*), but not in CD8αα IELs (Fig. 8, F to H). In addition, a higher proportion of *Taz*-deficient CD4 and CD8 T cells produced IFNγ compared with controls (Fig. 8, I and J). In line with the observations made at early IEL activation whereby the absence of Taz resulted in reduced IEL activity, Ev infection resulted in increased parasite burden with potential risk to immunopathology with the influx of activated CD4 and CD8 T cells in the absence of Taz compared with controls (*43*, *44*). These results highlight the particular importance of the mitochondria and their CL composition in rapid IEL effector release, which help to contain microbial threats, thereby reducing additional immune cell activation and risk of immunopathology.

DISCUSSION

Our results are consistent with the hypothesis that IELs are maintained in a controlled activation state. This state differs markedly from the quiescent state of naive and memory T cells and facilitates rapid effector function release, thereby reducing the amplitude of the adaptive immune response required to contain and clear invading microbes (*13*, *14*, *21*). The increased presence of proteins involved in lipid metabolism in IELs compared with conventional T cells suggested that altered metabolic processes, such as FAO, might be involved in maintaining the IEL activation status (*13*, *14*). We show that metabolism of IELs reflects that of recently activated T cells, but their metabolic capacity is curtailed to arrest them in a poised state similar to recently activated T cell storing lipids (*16*). We show that the poised activation mode correlates with alterations in IEL mitochondria and the mitochondrial membrane composition and show that IEL activation capacity is directly affected by alterations in CLs, which affects the ability of microbial control, suggesting a role of mitochondrial membrane dynamics in the activation of epithelial lymphocytes.

T cell activation requires significant metabolic reprogramming to re-enter cell cycle and produce effector molecules (*45*). Quantitative bioenergetic differences, such as mitochondrial mass, may contribute to more rapid induction of glycolysis and cell proliferation upon activation of memory T cells compared with naive T cells (*46*). In agreement, we found increased CL levels, mitochondrial numbers, and SRC in memory T cells compared with naive T cells. Altered mitochondrial function does not restrict steady-state IEL activity such as basal respiration, survival, and epithelial cell surveillance (*4*), but IEL effector functions directly correlated with the CL makeup of their mitochondria. CLs are important in the generation of an electrochemical gradient used to produce energy, such as across inner mitochondrial membrane (*30*). Transfer of ATP to the cytosol requires tetralinoleoyl CL (C72:8) (*47*, *48*). Furthermore, CLs are an active component of cytochrome c oxidase, required for electron transport and proton translocation (*49*), are essential for complex III function, and may play a role in complexes I, II, and V, participating in structural organization and stabilization of the respiratory chain complexes, thereby influencing supercomplex formation and function (*30*). The increased numbers of mitochondria in IELs did not result in increased metabolic potential. The absence of SRC in IELs and the altered CL composition of the mitochondrial membrane suggest a metabolic block in generating energy

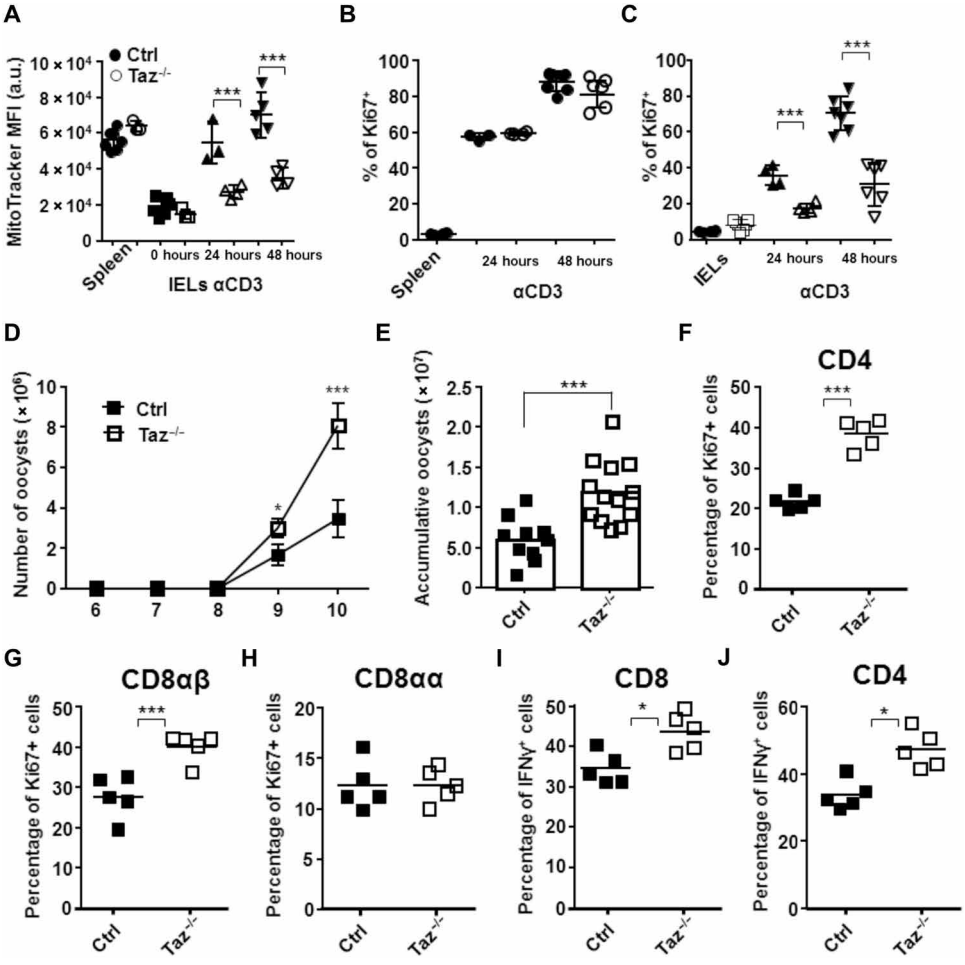

Fig. 8. Altered CL directly affects IEL function. C57BL/6 Rag2-deficient mice were reconstituted with wild-type control (closed symbols) or Tafazzin-deficient (open symbols) bone marrow. (**A** to **J**) Six to 8 weeks afterward, mice were injected intraperitoneally with anti-CD3 and $CD8^+$ T cells from the intestinal IEL compartment (A and C) or the spleen (B) were assessed at indicated time points for (A) MitoTracker Green or (B and C) Ki67 (three biological repeats with $n = 2$ to 3). Six to 8 weeks after bone marrow chimeric generation, mice were challenged with 1000 Ev oocysts, and (D) parasite load was assessed for the first 10 days daily or (E) accumulative load of shedded oocysts (accumulated from two biological repeats, $n = 5$ to 6). At day 10 postinfection, cells from the ileum IEL compartment were stained for Ki67 in (F) $CD4^+$ T cells, (G) $CD8\alpha\beta^+$ T cells, and (H) $CD8\alpha\alpha^+$ T cells. Furthermore, the IFNγ production in (I) $CD8^+$ or (**J**) $CD4^+$ T cells was assessed via intracellular staining (representative of two biological repeats with $n = 5$). Error bars indicate SDs. For statistics, multiple *t* test was used. $^*P < 0.05$, $^{**}P < 0.01$, $^{***}P < 0.001$.

levels required for clonal expansion and effector function. This prevents the progression of epithelial T cells to full effector function and to a quiescent memory cell state but may enable rapid activation (*50*). The altered CL composition in IELs is strongly associated with reduction of full mitochondrial activity. We show that the CL composition is dynamic and changes in line with other lymphocytes upon inflammatory signals, releasing IEL effector functions such as proliferation and ROS and cytokine production. The absence of *Tafazzin* specifically affects the early activation potential of IELs, not those of splenic T cells. Although there are limited data regarding immune effects in Barth syndrome patients, reported episodic diarrhea and constipation suggest gastrointestinal problems that may relate to altered immune function (*51*, *52*).

It remains to be determined how alterations in CL composition and Taz activity release or license IEL activity, which was not addressed in the current study. Biochemical analysis of isolated mitochondria may provide insights into alterations of membrane structure, mitochondrial structure, and function. It is highly likely that additional mitochondrial membrane modifications, not currently assessed, play a role in IEL biology. Although the CL composition of IELs is altered and important for IEL activation, additional metabolic or membrane compositional alterations in IELs are likely to play an important role. In the absence of Taz, the MitoTracker dye fluorescence intensity remained low compared with spleen T cells, indicating that alterations in CL are not solely or directly responsible for the low MitoTracker intensity.

The tight regulation of IEL activity is in line with a balanced immune surveillance and activity required at the epithelial barrier (*2*). The high burden of microbial and xenobiotic encounters, many of which are innocuous, requires restrained to prevent immunopathology. However, swift action is needed to contain invading microorganisms, thereby reducing the requirement of additional immune cell activation (*53*). Thus, alterations in mitochondrial membrane composition highlight an alternative mechanism enabling control of T cells in a heightened activation state. This mechanism may be especially suited to contribute to maximizing immune responses and minimizing immunopathology at the fragile epithelial barrier.

MATERIALS AND METHODS

Mice

C57BL/6J, IL-22–deficient (*54*), Rag2-deficient, and Rag2,IL2Rγc–double-deficient mice (the Jackson Laboratory) were bred at the Instituto de Medicina Molecular, Lisbon, Portugal, and at the Babraham Institute, Cambridge, UK. Taz-deficient mice were obtained from the Beatson Institute (*41*). Male and female mice at 8 to 14 weeks of age, unless otherwise specified, were used. Animals were housed in individually ventilated cages under temperature-controlled conditions and a 12-hour light/dark cycle with free access to drinking water and food. All mice were kept under specific pathogen–free conditions. Bone marrow chimeras were generated by sublethal irradiation (4.5 Gy) of Rag2-deficient mice and subsequent intravenous injection of bone marrow cells obtained. Antibiotic treatment (ampicillin, colistin, and streptomycin) was administered via drinking water (1 g/liter) for 10 to 14 days. Anti-CD3 was given intraperitoneally at 25 μg per animal. All animal experimentation complied with regulations of the Direção-Geral de Alimentação e Veterinária Portugal, the U.K. Home Office, and local ethical review committees and guidelines.

T cell isolation

Intestinal IELs were isolated as previously described (*42*). Spleens were mashed through a 70-μm strainer, and cells were lysed with red blood cell lysis buffer. IEL single-cell suspensions were further purified using 37.5% isotonic Percoll. Cells were used for analysis or purified by pre-enrichment for CD8α by autoMACS and BD Influx or FACSAria III. Care was taken not to touch the TCR, and TCRαβ or TCRγδ IELs were sorted by negative selection in separate runs. Cell viability, assessed by LIVE/DEAD dye or 4′,6-diamidino-2-phenylindole (DAPI) (cell sorting and flow cytometry) or by trypan blue staining (before Seahorse, microscopy, and mass spectrometry analysis), for all samples was higher than 95%. For adoptive transfers, 1×10^5 to 2×10^5 purified IELs were transferred intravenously, and $CD8^+$ T cells were purified by autoMACS (Miltenyi Biotec) and by flow cytometry (BD Influx or FACSAria III) (naive: $CD8^+CD44^{lo}CD62L^{hi}$; memory: $CD8^+CD44^{hi}$). For activation assays, cells were plated in wells coated with anti-CD3 (1 μg/ml) and anti-CD28 (3 μg/ml) together with IL-2 (5 ng/ml) for 2 days. Cells were resuspended and cultured in the absence of anti-CD3/CD28 in rmIL-2 (PeproTech).

Flow cytometry

Surface staining and sorting were performed according to the latest guidelines (*55*) and gating strategy shown in fig. S1C. Briefly, IELs or splenocytes were resuspended in phosphate-buffered saline (PBS) and stained with fluorescence-conjugated monoclonal antibodies for TCRγδ, TCRβ, CD4, CD8β, CD8α, and/or CD44 and L10119 LIVE/DEAD Fixable Near-IR staining (Invitrogen). All fluorochrome-conjugated monoclonal antibodies were purchased from BioLegend, except for anti-Tom20 and anti-Ki67 (BD Biosciences). Before surface staining, cells were stained for MitoTracker Green (M7514), MitoTracker Deep Red (M22426), MitoTracker Orange (M7510), MitoSOX Red, tetramethylrhodamine, ethyl ester, or Lysotracker red (all from Thermo Fisher Scientific); lipid droplet (Cayman's Lipid Droplets Fluorescence Assay Kit); or NAO (40 nM, Sigma-Aldrich), according to the manufacturers' instructions. For intracellular detection, cells were activated for 2 hours with phorbol 12,13-dibutyrate (500 ng/ml) and ionomycin (500 ng/ml) in the presence of Brefeldin A (1 μg/ml; all from Sigma-Aldrich) and subsequently stained with anti-TNF or anti-IFNγ fluorescence-conjugated antibodies. Anti-Ki67 was used according to the manufacturer's instructions.

Imaging

Skin samples were stained, as described before (*56*). Epidermal sheets were washed in PBS and blocked in 2% (w/v) bovine serum albumin before antibodies were added directly. Sheets were mounted onto silane-coated slides. Monoclonal antibodies used were panTCRγδ (GL3, BioLegend) and TCRVγ3 (536, BioLegend). FACSorted (fluorescence-activated cell sorted) T cells were stained for MitoTracker Green (Invitrogen) and DAPI. To identify lipid droplets, we stained cells with Nile Red (Cayman's Lipid Droplets Fluorescence Assay Kit) or LD540 dye (*57*) and DAPI. Confocal images were obtained using a Zeiss LSM 780 confocal microscope. Images were analyzed using the Zeiss LSM software.

Transmission electron microscopy

We FACSorted 2.5×10^6 naive ($CD44^{lo}$) or memory ($CD44^{hi}$) $CD8\alpha^+$ lymphocytes from the spleen and $CD8\alpha^+$ lymphocytes from the small intestinal epithelium (IELs) pooled from 10 sex- and age-matched mice. Cells were washed 2× in sodium cacodylate buffer, pelleted,

and fixed at 4°C in 2% glutaraldehyde/4% paraformaldehyde in 0.1 M cacodylate buffer overnight. Briefly, cells were postfixed with 1% osmium tetroxide in 0.1 M cacodylate buffer for 1 hour and dehydrated in a solution series containing 25 to 100% ethanol and 100% propylene oxide. Samples were embedded in Spurr's resin at 60°C for 24 hours. Ninety-nanometer sections were cut by Reichert-Jung Ultracut E, subsequently stained with uranyl acetate and lead citrate, and examined under 300 kV with a FEI Tecnai F30 transmission electron microscope. Images were photographed using a Gatan CCD digital micrograph with a 4k × 4k resolution.

Metabolism assay

OCRs and ECARs were obtained by culturing cells in XF media [nonbuffered Dulbecco's modified Eagle's medium (Sigma-Aldrich) containing 25 mM glucose, 2 mM L-glutamine, 1 mM sodium pyruvate, and 2% fetal bovine serum] under basal conditions and in response to 2.5 μM oligomycin, 0.5 μM FCCP, and 1 μM rotenone with 1 μM antimycin A (Sigma-Aldrich) on a Seahorse XF-24 analyzer.

Library preparation for RNA-seq

RNA sequencing (RNA-seq) libraries were constructed using the Tru-Seq sample preparation kit (Illumina), from polyA+ RNAs isolated from purified T cells. RNA libraries were run on the Bioanalyzer for quality control to check purity and size range. RNA-seq was performed on the Hi-Seq 2500 using a 100–base pair read length program. The barcoded samples were first demultiplexed and trimmed with the "cutadapt version 1.1" adapter removal software, using the following parameters: -f fastq -e 0.1 -q 20 -O 1 -a AGATCGGAAGAGC. For the mapping, we used the Ensembl GRCm38 genome annotation together with "TopHat" alignment software, where more than 95% of all complementary DNAs were mapped to the reference genome. Differential expression analysis was carried out comparing CD8 subsets. All normalizations and differential expression analysis were performed in R (version 3.1.0) together with the DESeq2 Bioconductor package and the Negative Binomial Distribution method (*58*). Differentially expressed genes were selected by significance of adjusted *P* value that was lower than 0.05.

Eimeria infection

E. vermiformis oocysts not older than 4 months and stored in 2.5% potassium bichromate were used for infection of 8- to 14-week-old mice. Oocysts were washed three times with deionized water (1800*g*, 8 min) and subsequently flotated (1100*g*, 10 min) and sterilized using sodium hypochloride. After three washes with deionized water, oocysts were quantified with a Fuchs-Rosenthal chamber. To exactly adjust low doses, we screened a 50-μl droplet of the oocyst suspension in a McMaster chamber. One thousand oocysts were inoculated via oral gavage in a volume of 100 to 150 μl of water.

Lipidomics

Cell pellets were resuspended in 1.5 ml of methanol and thoroughly mixed with 1.5 ml of water and 3 ml of chloroform via vortex. Two hundred nanograms of 14:0/14:0/14:0/14:0-cardiolipin (56:0-CL) was spiked to each sample before Folch extraction as internal standard. Lower phase was concentrated with SpeedVac at room temperature and redissolved in 100 μl of chloroform. Seventeen microliters of chloroform solution was injected for liquid chromatography–mass spectrometry (LC-MS) analysis. Different classes of lipids were separated via normal phase high-performance liquid chromatography on a MicroSolv Type C silica column with the Shimadzu Prominence system. Different lipid molecular species in each class were analyzed with a Thermo Orbitrap Elite mass spectrometer. Specifically, the analysis of CL was carried out on SIM mode with FT-MS [mass range, 560 to 880 mass/charge ratio (m/z); mass resolution, 240k at 400 m/z; mass accuracy, ~3 parts per million]. All the lipid standards are from Avanti Polar Lipids. All the solvents for lipid extraction and analysis are LC-MS grade from Thermo Fisher Scientific.

Statistical analysis

P values were calculated using one-way analysis of variance (ANOVA) with multiple comparison test, regression test, or unpaired *t* test, as indicated in the figure legends after initial D'agostino-Pearson normality test. Differences were considered statistically significant with $P < 0.05$. Significance is indicated as follows: $*P < 0.05$, $**P < 0.01$, and $***P < 0.001$.

SUPPLEMENTARY MATERIALS

immunology.sciencemag.org/cgi/content/full/3/24/eaan2543/DC1

Fig. S1. IELs are a homogeneous population based on surface activation markers.
Fig. S2. LAMP-1 staining in $CD8^+$ T cells.
Fig. S3. IELs are maintained and contain increased numbers of mitochondria.
Fig. S4. IELs have altered mitochondrial staining.
Fig. S5. IEL mitochondrial staining correlates with activation.
Fig. S6. IEL mitochondria have altered CL composition.
Fig. S7. CL species distribution in T lymphocytes.
Fig. S8. Tafazzin is important in IEL activation.
Table S1. Characteristics of IELs compared with naive, effector, and memory $CD8^+$ T cells.
Table S2. Raw data (Excel).

REFERENCES AND NOTES

1. R. J. Cieza, A. T. Cao, Y. Cong, A. G. Torres, Immunomodulation for gastrointestinal infections. *Expert Rev. Anti Infect. Ther.* **10**, 391–400 (2012).
2. E. Moens, M. Veldhoen, Epithelial barrier biology: Good fences make good neighbours. *Immunology* **135**, 1–8 (2012).
3. H. Cheroutre, F. Lambolez, D. Mucida, The light and dark sides of intestinal intraepithelial lymphocytes. *Nat. Rev. Immunol.* **11**, 445–456 (2011).
4. A. Zaid, L. K. Mackay, A. Rahimpour, A. Braun, M. Veldhoen, F. R. Carbone, J. H. Manton, W. R. Heath, S. N. Mueller, Persistence of skin-resident memory T cells within an epidermal niche. *Proc. Natl. Acad. Sci. U.S.A.* **111**, 5307–5312 (2014).
5. D. Masopust, J. M. Schenkel, The integration of T cell migration, differentiation and function. *Nat. Rev. Immunol.* **13**, 309–320 (2013).
6. J. E. Knickelbein, K. M. Khanna, M. B. Yee, C. J. Baty, P. R. Kinchington, R. L. Hendricks, Noncytotoxic lytic granule–mediated $CD8^+$ T cell inhibition of HSV-1 reactivation from neuronal latency. *Science* **322**, 268–271 (2008).
7. D. Masopust, V. Vezys, A. L. Marzo, L. Lefrançois, Preferential localization of effector memory cells in nonlymphoid tissue. *Science* **291**, 2413–2417 (2001).
8. D. A. Hildeman, Y. Zhu, T. C. Mitchell, P. Bouillet, A. Strasser, J. Kappler, P. Marrack, Activated T cell death in vivo mediated by proapoptotic Bcl-2 family member bim. *Immunity* **16**, 759–767 (2002).
9. L. V. Sinclair, J. Rolf, E. Emslie, Y.-B. Shi, P. M. Taylor, D. A. Cantrell, Control of amino-acid transport by antigen receptors coordinates the metabolic reprogramming essential for T cell differentiation. *Nat. Immunol.* **14**, 500–508 (2013).
10. V. Abadie, V. Discepolo, B. Jabri, Intraepithelial lymphocytes in celiac disease immunopathology. *Semin. Immunopathol.* **34**, 551–566 (2012).
11. A. Regnault, A. Cumano, P. Vassalli, D. Guy-Grand, P. Kourilsky, Oligoclonal repertoire of the CD8 alpha alpha and the CD8 alpha beta TCR-alpha/beta murine intestinal intraepithelial T lymphocytes: Evidence for the random emergence of T cells. *J. Exp. Med.* **180**, 1345–1358 (1994).
12. A. Hayday, E. Theodoridis, E. Ramsburg, J. Shires, Intraepithelial lymphocytes: Exploring the Third Way in immunology. *Nat. Immunol.* **2**, 997–1003 (2001).
13. A. M. Fahrer, Y. Konigshofer, E. M. Kerr, G. Ghandour, D. H. Mack, M. M. Davis, Y.-h. Chien, Attributes of γδ intraepithelial lymphocytes as suggested by their transcriptional profile. *Proc. Natl. Acad. Sci. U.S.A.* **98**, 10261–10266 (2001).
14. J. Shires, E. Theodoridis, A. C. Hayday, Biological insights into $TCR\gamma\delta^+$ and $TCR\alpha\beta^+$ intraepithelial lymphocytes provided by serial analysis of gene expression (SAGE). *Immunity* **15**, 419–434 (2001).

15. Y. Zhang, Q. Li, E. Rao, Y. Sun, M. E. Grossmann, R. J. Morris, M. P. Cleary, B. Li, Epidermal fatty acid binding protein promotes skin inflammation induced by high-fat diet. *Immunity* **42**, 953–964 (2015).
16. Y. Pan, T. Tian, C. O. Park, S. Y. Lofftus, S. Mei, X. Liu, C. Luo, J. T. O'Malley, A. Gehad, J. E. Teague, S. J. Divito, R. Fuhlbrigge, P. Puigserver, J. G. Krueger, G. S. Hotamisligil, R. A. Clark, T. S. Kupper, Survival of tissue-resident memory T cells requires exogenous lipid uptake and metabolism. *Nature* **543**, 252–256 (2017).
17. D. O'Sullivan, G. J. W. van der Windt, S. C.-C. Huang, J. D. Curtis, C.-H. Chang, M. D. Buck, J. Qiu, A. M. Smith, W. Y. Lam, L. M. DiPlato, F.-F. Hsu, M. J. Birnbaum, E. J. Pearce, E. L. Pearce, Memory $CD8^+$ T cells use cell-intrinsic lipolysis to support the metabolic programming necessary for development. *Immunity* **41**, 75–88 (2014).
18. K. L. Cepek, S. K. Shaw, C. M. Parker, G. J. Russell, J. S. Morrow, D. L. Rimm, Michael B. Brenner, Adhesion between epithelial cells and T lymphocytes mediated by E-cadherin and the $\alpha^E\beta7$ integrin. *Nature* **372**, 190–193 (1994).
19. A. S. Rambold, S. Cohen, J. Lippincott-Schwartz, Fatty acid trafficking in starved cells: Regulation by lipid droplet lipolysis, autophagy, and mitochondrial fusion dynamics. *Dev. Cell* **32**, 678–692 (2015).
20. J. C. Stinchcombe, E. Majorovits, G. Bossi, S. Fuller, G. M. Griffiths, Centrosome polarization delivers secretory granules to the immunological synapse. *Nature* **443**, 462–465 (2006).
21. R. Boismenu, W. L. Havran, Intraepithelial gamma delta T cells exposed by functional genomics. *Genome Biol.* **2**, reviews103.1 (2001).
22. S. R. Carding, P. J. Egan, γδ T cells: Functional plasticity and heterogeneity. *Nat. Rev. Immunol.* **2**, 336–345 (2002).
23. G. J. W. van der Windt, B. Everts, C.-H. Chang, J. D. Curtis, T. C. Freitas, E. A. Edward, J. P. Erika, L. Pearce, Mitochondrial respiratory capacity is a critical regulator of $CD8^+$ T cell memory development. *Immunity* **36**, 68–78 (2012).
24. M. D. Buck, D. O'Sullivan, R. I. K. Geltink, J. D. Curtis, C.-H. Chang, D. E. Sanin, J. Qiu, O. Kretz, D. Braas, G. J. W. van der Windt, Q. Chen, S. C.-C. Huang, C. M. O'Neill, B. T. Edelson, E. J. Pearce, H. Sesaki, T. B. Huber, A. S. Rambold, E. L. Pearce, Mitochondrial dynamics controls T cell fate through metabolic programming. *Cell* **166**, 63–76 (2016).
25. J. F. Keij, C. Bell-Prince, J. A. Steinkamp, Staining of mitochondrial membranes with 10-nonyl acridine orange, MitoFluor Green, and MitoTracker Green is affected by mitochondrial membrane potential altering drugs. *Cytometry* **39**, 203–210 (2000).
26. K. Inagaki-Ohara, F. N. Dewi, H. Hisaeda, A. L. Smith, F. Jimi, M. Miyahira, A. S. F. Abdel-Aleem, Yoichiro Horii, Yukifumi Nawa,Intestinal intraepithelial lymphocytes sustain the epithelial barrier function against *Eimeria vermiformis* infection. *Infect. Immun.* **74**, 5292–5301 (2006).
27. A. L. Smith, A. C. Hayday, An αβ T-cell-independent immunoprotective response towards gut coccidia is supported by γδ cells. *Immunology* **101**, 325–332 (2000).
28. G. F. Sonnenberg, L. A. Fouser, D. Artis, Border patrol: Regulation of immunity, inflammation and tissue homeostasis at barrier surfaces by IL-22. *Nat. Immunol.* **12**, 383–390 (2011).
29. M. Schlame, S. Brody, K. Y. Hostetler, Mitochondrial cardiolipin in diverse eukaryotes. Comparison of biosynthetic reactions and molecular acyl species. *Eur. J. Biochem.* **212**, 727–733 (1993).
30. G. Paradies, V. Paradies, V. De Benedictis, F. M. Ruggiero, G. Petrosillo, Functional role of cardiolipin in mitochondrial bioenergetics. *Biochim. Biophys. Acta* **1837**, 408–417 (2014).
31. V. Koshkin, M. L. Greenberg, Cardiolipin prevents rate-dependent uncoupling and provides osmotic stability in yeast mitochondria. *Biochem. J.* **364**, 317–322 (2002).
32. E. Mileykovskaya, W. Dowhan, R. L. Birke, D. Zheng, L. Lutterodt, T. H. Haines, Cardiolipin binds nonyl acridine orange by aggregating the dye at exposed hydrophobic domains on bilayer surfaces. *FEBS Lett.* **507**, 187–190 (2001).
33. A. J. Chicco, G. C. Sparagna, Role of cardiolipin alterations in mitochondrial dysfunction and disease. *Am. J. Physiol. Cell Physiol.* **292**, C33–C44 (2007).
34. R. H. Houtkooper, F. M. Vaz, Cardiolipin, the heart of mitochondrial metabolism. *Cell. Mol. Life. Sci.* **65**, 2493–2506 (2008).
35. M. Schlame, M. Ren, Y. Xu, M. L. Greenberg, I. Haller, Molecular symmetry in mitochondrial cardiolipins. *Chem. Phys. Lipids* **138**, 38–49 (2005).
36. F. L. Hoch, Cardiolipins and biomembrane function. *Biochim. Biophys. Acta* **1113**, 71–133 (1992).
37. A. L. Duncan, A. J. Robinson, J. E. Walker, Cardiolipin binds selectively but transiently to conserved lysine residues in the rotor of metazoan ATP synthases. *Proc. Natl. Acad. Sci. U.S.A.* **113**, 8687–8692 (2016).
38. M. Schlame, J. A. Towbin, P. M. Heerdt, R. Jehle, S. DiMauro, T. J. J. Blanck MD, Deficiency of tetralinoleoyl-cardiolipin in Barth syndrome. *Ann. Neurol.* **51**, 634–637 (2002).
39. M. Schlame, D. Acehan, B. Berno, Y. Xu, S. Valvo, M. Ren, D. L Stokes, R. M. Epand, The physical state of lipid substrates provides transacylation specificity for tafazzin. *Nat. Chem. Biol.* **8**, 862–869 (2012).
40. R. H. Houtkooper, R. J. Rodenburg, C. Thiels, H. van Lenthe, F. Stet, B. T. Poll-The, J. E. Stone, C. G. Steward, R. J. Wanders, J. Smeitink, W. Kulik, F. M. Vaz, Cardiolipin and monolysocardiolipin analysis in fibroblasts, lymphocytes, and tissues using high-performance liquid chromatography-mass spectrometry as a diagnostic test for Barth syndrome. *Anal. Biochem.* **387**, 230–237 (2009).
41. L. C. Cadalbert, F. N. Ghaffar, D. Stevenson, S. Bryson, F. M. Vaz, E. Gottlieb, D. Strathdee, Mouse tafazzin is required for male germ cell meiosis and spermatogenesis. *PLOS ONE* **10**, e0131066 (2015).
42. Y. Li, S. Innocentin, D. R. Withers, N. A. Roberts, A. R. Gallagher, E. F. Grigorieva, C. Wilhelm, M. Veldhoen, Exogenous stimuli maintain intraepithelial lymphocytes via aryl hydrocarbon receptor activation. *Cell* **147**, 629–640 (2011).
43. E. Ramsburg, R. Tigelaar, J. Craft, A. Hayday, Age-dependent requirement for γδ T cells in the primary but not secondary protective immune response against an intestinal parasite. *J. Exp. Med.* **198**, 1403–1414 (2003).
44. S. J. Roberts, A. L. Smith, A. B. West, L. Wen, R. C. Findly, M. J. Owen, A. C. Hayday, T-cell alpha beta + and gamma delta + deficient mice display abnormal but distinct phenotypes toward a natural, widespread infection of the intestinal epithelium. *Proc. Natl. Acad. Sci. U.S.A.* **93**, 11774–11779 (1996).
45. S. E. Hamilton, S. C. Jameson, CD8 T cell quiescence revisited. *Trends Immunol.* **33**, 224–230 (2012).
46. G. J. W. van der Windt, D. O'Sullivan, B. Everts, S. C.-C. Huang, M. D. Buck, J. D. Curtis, C.-H. Chang, A. M. Smith, T. Ai, B. Faubert, R. G. Jones, E. J. Pearce, E. L. Pearce, CD8 memory T cells have a bioenergetic advantage that underlies their rapid recall ability. *Proc. Natl. Acad. Sci. U.S.A.* **110**, 14336–14341 (2013).
47. H. Nury, C. Dahout-Gonzalez, V. Trézéguet, G. J. M. Lauquin, G. Brandolin, E. Pebay-Peyroula, Relations between structure and function of the mitochondrial ADP/ATP carrier. *Annu. Rev. Biochem.* **75**, 713–741 (2006).
48. M. Klingenberg, Cardiolipin and mitochondrial carriers. *Biochim. Biophys. Acta* **1788**, 2048–2058 (2009).
49. E. Sedlák, N. C. Robinson, Phospholipase A_2 digestion of cardiolipin bound to bovine cytochrome *c* oxidase alters both activity and quaternary structure. *Biochemistry* **38**, 14966–14972 (1999).
50. S. N. Mueller, L. K. Mackay, Tissue-resident memory T cells: Local specialists in immune defence. *Nat. Rev. Immunol.* **16**, 79–89 (2016).
51. C. Ferreira, R. Thompson, H. Vernon, in *GeneReviews®*, M. P. Adam, H. H. Ardinger, R. A. Pagon, S. E. Wallace, L. J. H. Bean, K. Stephens, A. Amemiya, Eds. (University of Washington, 1993).
52. S. L. N. Clarke, A. Bowron, I. L. Gonzalez, S. J. Groves, R. Newbury-Ecob, N. Clayton, R. P. Martin, B. Tsai-Goodman, V. Garratt, M. Ashworth, V. M. Bowen, K. R. McCurdy, M. K. Damin, C. T. Spencer, M. J. Toth, R. I. Kelley, C. G. Steward, Barth syndrome. *Orphanet J. Rare Dis.* **8**, 23 (2013).
53. Š. Konjar, C. Ferreira, B. Blankenhaus, M. Veldhoen, Intestinal barrier interactions with specialized CD8 T cells. *Front. Immunol.* **8**, 1281 (2017).
54. K. Kreymborg, R. Etzensperger, L. Dumoutier, S. Haak, A. Rebollo, T. Buch, F. L. Heppner, J.-C. Renauld, B. Becher, IL-22 is expressed by Th17 cells in an IL-23-dependent fashion, but not required for the development of autoimmune encephalomyelitis. *J. Immunol.* **179**, 8098–8104 (2007).
55. A. Cossarizza, H.-D. Chang, A. Radbruch, M. Akdis, I. Andrä, F. Annunziato, P. Bacher, V. Barnaba, L. Battistini, W. M. Bauer, S. Baumgart, B. Becher, W. Beisker, C. Berek, A. Blanco, G. Borsellino, P. E. Boulais, R. R. Brinkman, M. Büscher, D. H. Busch, T. P. Bushnell, X. Cao, A. Cavani, P. K. Chattopadhyay, Q. Cheng, S. Chow, M. Clerici, A. Cooke, A. Cosma, L. Cosmi, A. Cumano, V. Duc Dang, D. Davies, S. De Biasi, G. Del Zotto, S. Della Bella, P. Dellabona, G. Deniz, M. Dessing, A. Diefenbach, J. Di Santo, F. Dieli, A. Dolf, V. S. Donnenberg, T. Dörner, G. R. A. Ehrhardt, E. Endl, P. Engel, B. Engelhardt, C. Esser, B. Everts, A. Dreher, C. S. Falk, T. A. Fehniger, A. Filby, S. Fillatreau, M. Follo, I. Förster, J. Foster, G. A. Foulds, P. S. Frenette, D. Galbraith, N. Garbi, M. Dolores García-Godoy, J. Geginat, K. Ghoreschi, L. Gibellini, C. Goettlinger, C. S. Goodyear, A. Gori, J. Grogan, M. Gross, A. Grützkau, D. Grummitt, J. Hahn, Q. Hammer, A. E. Hauser, D. L. Haviland, D. Hedley, G. Herrera, M. Herrmann, F. Hiepe, T. Holland, P. Hombrink, J. P. Houston, B. F. Hoyer, B. Huang, C. A. Hunter, A. Iannone, H.-M. Jäck, B. Jávega, S. Jonjic, K. Juelke, S. Jung, T. Kaiser, T. Kalina, B. Keller, S. Khan, D. Kienhöfer, T. Kroneis, D. Kunkel, C. Kurts, P. Kvistborg, J. Lannigan, O. Lantz, A. Larbi, S. LeibundGut-Landmann, M. D. Leipold, M. K. Levings, V. Litwin, Y. Liu, M. Lohoff, G. Lombardi, L. Lopez, A. Lovett-Racke, E. Lubberts, B. Ludewig, E. Lugli, H. T. Maecker, G. Martrus, G. Matarese, C. Maueröder, M. McGrath, I. McInnes, H. E. Mei, F. Melchers, S. Melzer, D. Mielenz, K. Mills, D. Mirrer, J. Mjösberg, J. Moore, B. Moran, A. Moretta, L. Moretta, T. R. Mosmann, S. Müller, W. Müller, C. Münz, G. Multhoff, L. Enrique Munoz, K. M. Murphy, T. Nakayama, M. Nasi, C. Neudörfl, J. Nolan, S. Nourshargh, J.-E. O'Connor, W. Ouyang, A. Oxenius, R. Palankar, I. Panse, P. Peterson, C. Peth, J. Petriz, D. Philips, W. Pickl, S. Piconese, M. Pinti, A. Graham Pockley, M. Justyna Podolska, C. Pucillo, S. A. Quataert, T. R. D. J. Radstake, B. Rajwa, J. A. Rebhahn, D. Recktenwald, E. B. M. Remmerswaal, K. Rezvani, L. G. Rico, J. Paul Robinson, C. Romagnani, A. Rubartelli, B. Ruckert, J. Ruland, S. Sakaguchi, F. Sala-de-Oyanguren, Y. Samstag, S. Sanderson, B. Sawitzki, A. Scheffold, M. Schiemann, F. Schildberg, E. Schimisky, S. A. Schmid, S. Schmitt, K. Schober, T. Schüler, A. Ronald Schulz, T. Schumacher, C. Scotta, T. Vincent Shankey, A. Shemer, A.-K. Simon,

J. Spidlen, A. M. Stall, R. Stark, C. Stehle, M. Stein, T. Steinmetz, H. Stockinger, Y. Takahama, A. Tarnok, Z. G. Tian, G. Toldi, J. Tornack, E. Traggiai, J. Trotter, H. Ulrich, M. van der Braber, R. A. W. van Lier, M. Veldhoen, S. Vento-Asturias, P. Vieira, D. Voehringer, H.-D. Volk, K. von Volkmann, A. Waisman, R. Walker, M. D. Ward, K. Warnatz, S. Warth, J. V. Watson, C. Watzl, L. Wegener, A. Wiedemann, J. Wienands, G. Willimsky, J. Wing, P. Wurst, L. Yu, A. Yue, Q. Zhang, Y. Zhao, S. Ziegler, J. Zimmermann, Guidelines for the use of flow cytometry and cell sorting in immunological studies. *Eur. J. Immunol.* **47**, 1584–1797 (2017).

56. P. R. Bergstresser, D. V. Juarez, Detection by immunochemical techniques of cell surface markers on epidermal Langerhans cells. *Methods Enzymol.* **108**, 683–691 (1984).
57. J. Spandl, D. J. White, J. Peychl, C. Thiele, Live cell multicolor imaging of lipid droplets with a new dye, LD540. *Traffic* **10**, 1579–1584 (2009).
58. M. I. Love, W. Huber, S. Anders, Moderated estimation of fold change and dispersion for RNA-seq data with DESeq2. *Genome Biol.* **15**, 550 (2014).

Acknowledgments: We acknowledge the assistance of the Biological Services, Lipidomics, Imaging, and Flow Cytometry facilities at the Instituto de Medicina Molecular and Babraham Institute. We thank Y. Chen (Electron Microscopy facility, University of Chicago) for assistance with transmission electron microscopy (TEM), U. Vrhovšek for preliminary lipidomic analysis (Fondazione Edmund Mach, San Michele All'adige), and V. Morais and F. Carvalho for help with the Seahorse and reagents. **Funding:** This work was supported by the U.S. NIH (R01DK67180) for work in the Jabri laboratory; the Agency for Science, Technology and Research (to Y.L.); the European Research Council (no. 280307-Epithelial_Immunol); the Biotechnology and Biological Sciences Research Council (BBS/E/B/000C0407 and BBS/E/B/000C0409); NC3R (NC/L001217/1); and the European Union H2020 ERA project (no. 667824-EXCELLtoINNOV) for work in the M. Veldhoen laboratories. Publication costs were provided by LISBOA-01-0145-FEDER-007391, projeto cofinanciado pelo FEDER através POR Lisboa 2020-Programa Operacional Regional de Lisboa, do PORTUGAL 2020, e pela Fundação para a Ciência e a Tecnologia. **Author contributions:** M.V. and Š.K. conceived the project. Š.K. performed microscopy, mRNA sequencing, Seahorse, and flow cytometry studies; performed statistical analysis; and analyzed and interpreted the data. U.C.F. performed flow cytometry studies and statistical analysis and analyzed and interpreted the data. R.H. and T.M. performed TEM studies and analysis. C.F. with J.G. performed *E. vermiformis* studies and flow cytometry and analyzed and interpreted the data. B.B. generated bone marrow chimeras and provided assistance. Y.L. performed skin analysis. M.B. and S.I. assisted with the experiments. Q.Z. analyzed the CLs. N.H. performed the bioinformatics analysis. J.S. provided *E. vermiformis*. D.S. supplied the TazKO mouse. B.J. and M.V. coordinated the research. M.V. directed the research and wrote the manuscript with input from co-authors. **Competing interests:** The authors declare that they have no competing financial interests. **Data and materials availability:** The data for this study have been deposited in the database ArrayExpress, with accession number E-MTAB-6510.

Submitted 17 March 2017
Resubmitted 19 October 2017
Accepted 24 April 2018
Published 22 June 2018
10.1126/sciimmunol.aan2543

Citation: Š. Konjar, U. C. Frising, C. Ferreira, R. Hinterleitner, T. Mayassi, Q. Zhang, B. Blankenhaus, N. Haberman, Y. Loo, J. Guedes, M. Baptista, S. Innocentin, J. Stange, D. Strathdee, B. Jabri, M. Veldhoen, Mitochondria maintain controlled activation state of epithelial-resident T lymphocytes. *Sci. Immunol.* **3**, eaan2543 (2018).

Science Immunology

Mitochondria maintain controlled activation state of epithelial-resident T lymphocytes

Spela Konjar, Ulrika C. Frising, Cristina Ferreira, Reinhard Hinterleitner, Toufic Mayassi, Qifeng Zhang, Birte Blankenhaus, Nejc Haberman, Yunhua Loo, Joana Guedes, Marta Baptista, Silvia Innocentin, Joerg Stange, Douglas Strathdee, Bana Jabri and Marc Veldhoen

Sci. Immunol. **3**, eaan2543.
DOI: 10.1126/sciimmunol.aan2543

Controlled activation

At the intestinal barrier, lymphocyte activation is a tightly regulated process that enables rapid responses to pathogens but avoids destructive inflammation. Konjar *et al*. examine how intraepithelial lymphocytes (IELs) maintain a controlled activation state, which is influenced by the composition of the mitochondrial membrane. Inflammation triggers changes in the mitochondrial membranes of IELs, particularly the cardiolipin composition, and these changes support rapid proliferation and effector functions. These findings reveal a role for mitochondria in controlling the activation state of IELs, thus furthering our insights into how mitochondria can influence immune responses.

Science Immunology (ISSN 2470-9468) is published by the American Association for the Advancement of Science, 1200 New York Avenue NW, Washington, DC 20005. The title *Science Immunology* is a registered trademark of AAAS.